Biomass Conversion and Biorefinery (2021) 11:1067–1083
https://doi.org/10.1007/s13399-020-01063-8

ORIGINAL ARTICLE

# Investigation of effectiveness of pine cone biochar activated with KOH for methyl orange adsorption and $CO_2$ capture

Nihan Kaya[1] · Zeynep Yıldız Uzun[2]

Received: 13 August 2020 / Revised: 24 September 2020 / Accepted: 2 October 2020 / Published online: 12 October 2020


## Abstract

In this study, pyrolysis of pine cone, a lignocellulosic biomass, was carried out in a fixed bed reactor. The biochar product obtained was activated by using chemical activation method. KOH was used as the activating agent with the impregnation ratio was ¼. Activated pine cone biochars were characterized by using analysis techniques such as SEM, BET, and FT-IR. The usage potential of the activated biochar product with a surface area of 1714.5 $m^2$/g has been investigated in two different application areas. As the first application area, the $CO_2$ holding capacity of activated biochar was measured by using the thermogravimetric analysis method. The $CO_2$ adsorption capacity of the activated biochar was determined as 160 mg/g (3.64 mmol/g) at 25 °C. As a second application area, the effectiveness of activated biochar product in the removal of dyestuff (methyl orange) from aqueous solutions was investigated. The methyl orange adsorption capacity of the activated biochar in optimum conditions (pH 2, temperature of 25 °C, initial concentration of 100 mg/L, adsorbent amount 0.8 g/L) was calculated as 109.5 mg/g. Isotherm modeling and kinetic investigations showed that Freundlich and pseudo-second-order models describe the adsorption equilibrium and kinetic behavior well. As a result, this type of biomass could be successfully evaluated in removing both methyl orange dye, which is a potential pollution risk for aquatic environment, and $CO_2$ that is responsible for climate change and greenhouse effect in the atmosphere.

**Keywords** Pine cone · Activated biochar · Pyrolysis · Adsorption · $CO_2$ capture · Methyl orange

## 1 Introduction

In recent years, biochars have been accepted as an important tool to improve environmental management and provide energy production. Biochar is a material formed as a result of the carbonization of biomass containing carbon. The most common definition of biochar made so far is stated as a solid material obtained as a result of thermochemical transformations of biomass in an environment where oxygen is limited. These products are potential candidates for sustainable energy production and environmental management. Biochar products are produced depending on different operating conditions and process parameters as a result of thermochemical processes. Therefore, the products have different physical and chemical properties. Characterization of the biochar is very important as it plays an important role in determining their applications in industrial and environmental management. For example, a biochar with low carbon content and high ash content is not suitable for the energy product. Likewise, it is not preferred to use biochar products with low surface area as adsorbent. The composition of the biomass used as raw material also has a direct effect on the physicochemical properties of the biochar produced by the thermochemical process. The composition of the biomass at temperatures above 180 °C undergoes a series of chemical reactions, and as a result, the molecular structure turns into an aromatic form with a high porous surface area. For example, biochars produced by pyrolysis at 350 °C have small amounts of alkyl-O, alkyl-C, and aromatic (aryl) carbons in their structure. When the reaction temperature is increased (> 500 °C), these alkyl-O and alkyl-C groups turn completely into aryl-C groups [1].

✉ Nihan Kaya
nihankaya@hitit.edu.tr

Zeynep Yıldız Uzun
zeynepyildiz.omu@gmail.com

[1] Engineering Faculty, Department of Chemical Engineering, Hitit University, Çorum, Turkey

[2] Boyabat Vocational School, Department of Chemistry and Chemical Processing Technologies, Sinop University, Sinop, Turkey

Biochar products are materials with a high surface area, large pore volume, and rich superficial functional groups and can be defined as products that have a wide range of applications compared with materials obtained after other chemical processes and that are cost-effective and can be easily prepared using different sources. Biochars have been used as adsorbent, catalyst, soil conditioner, and energy storage products in recent years [2]. Due to its low cost, porous structure, and high efficiency, biochar products are used as catalysts in energy generation, waste management, catalytic electrode materials, removal of environmental pollution, biomass hydrolysis, bio-oil improvement, and chemical production [2, 3]. However, biochars are also widely used as soil conditioners due to their special metal compositions and unique surface structure. Biochar products, which have benefits such as increasing the fertility of degraded soils, reducing toxicity from aluminum metal, and increasing biological activity, have been recognized as promising materials for improving or regulating soil contaminated with various pollutants, especially heavy metals and pesticides [2, 4]. Another usage area of biochar obtained as a result of thermochemical transformations of biomass is electrochemical energy storage applications. Electrochemical energy storage systems such as supercapacitors and lithium-ion batteries have attracted considerable attention in recent years. Carbon-based biochar products are also preferred in electrochemical energy storage devices due to their high surface area, wide pore distribution, high electrical conductivity, and strong mechanical properties. In this context, biochars are used as electrodes in supercapacitors [5, 6]. In addition to all these usage areas of biochars, researches on the use of biochar products as adsorbent to treat pollutants in the environment, especially in wastewater and emissions, are attracting much more attention from researchers. In particular, the use of carbon-containing agricultural by-products and residues as adsorbents for water treatment is low cost and easy to apply.

Air and water pollution are the leading environmental problems that have become a global problem from out of locality in the early 1970s. The air pollution problem, which is one of these types of pollution, which varies according to urbanization, industrialization, and population amount and has reached serious dimensions as a result of human activities, has become the most binding type of pollution that makes countries responsible to each other. Especially $CO_2$, which occurs as a result of burning fossil fuels and causes negative effects in the atmosphere, is a gas that creates a greenhouse effect and causes global warming. Considering not only the atmosphere but also the negative effects on living life, reducing the emission of $CO_2$ or removing carbon dioxide from the earth's atmosphere is of international importance. One of the methods used for this purpose is $CO_2$ storage; it is reported in the literature that activated carbons, carbon nanotubes, zeolites, metal-organic frameworks, etc. are commonly used as adsorbent materials for the capture of $CO_2$. In recent years, the production of effective adsorbent from agricultural wastes is gradually increasing. Creamer et al. (2014) produced biochars from sugar cane by pyrolysis process at different temperatures (300, 450, and 600 °C) and they used these biochar products for $CO_2$ storage at 25 °C. The results showed that biochar produced at high temperatures has the highest $CO_2$ storage capacity (73.55 mg/g at 25 °C). Also, when the specific surface area of the biochar is large enough, the amount of nitrogenous functional groups played an important role in the adsorption of $CO_2$ to the biochar surface [7].

Water pollution is another of today's environmental problems. Water is the natural resource which is the most affected by environmental pollution and the most vulnerable in terms of environmental pollution. Considering that the water resources required for life, economic development, and environment are limited, it is seen how important the issue is. In this context, it is of great importance that contaminated water, that is, the water whose natural composition is degraded especially as a result of industrial activities, is purified and released to nature. Dyestuffs are one of the most important environmental pollutants in water sources because of having a carcinogenic effect in living things and also they are resistant to environmental conditions depending on their low biodegradation rates [8]. Therefore, it is imperative to treat wastewater containing dyestuffs before they are released into nature. In recent years, many studies have been conducted on biochar production and their use as alternative adsorbents in water treatment by using carbon-containing agricultural by-products and wastes. Especially in removing the anionic and cationic dyes, which have a wide range of applications in the textile industry, from the aqueous environment, the use of biochars is becoming increasingly common as an important alternative to activated carbon in terms of its low cost and ease of application. In the literature, biochars were produced using coconut shells, olive kernel, cherry kernel, waste tea, almond peel, peach kernel peel, apricot kernel, cotton stalk, etc., and their adsorption capacities were investigated by determining their characteristics [9–12].

Activating biochars to be used for environmental purposes is another important issue and many methods have been developed for this purpose. These methods are divided into two main groups: chemical and physical activation. In recent years, chemical activation has been one of the most preferred methods. Chemical activation can be carried out using suitable acid, base, and metal salts. The main purpose of acid activation is to remove the unwanted metals from the structure and connect the functional groups in the acid to the biochar surface. Hydrochloric acid, sulfuric acid, nitric acid, phosphoric acid, oxalic acid, and citric acid are among the most used acids in the literature for acid activation. The main purpose of activation with the base is to increase the surface area of the biochar and the functional groups it contains. Common

compounds used for base activation are potassium hydroxide and sodium hydroxide [3]. For example, in the literature, it has been reported that both the surface area (from 14.4 to 49.1 $m^2$/g) and the functional groups in its structure have increased as a result of KOH activation of the biochar obtained by municipal solid waste pyrolysis [13]. In another study, it was reported that the surface area of the biochar activated by 1 M HCl increased from 58.75 to 88.35 $m^2$/g [14]. Generally, the basic activation of biomass with metal alkaline hydroxides such as KOH and NaOH causes the production of biochars with high surface areas that can reach up to 2000 $m^2$/g [15]. Especially, the surface of KOH-activated biochars, which may be used in the removal of a wide range of contaminants and carcinogenic compounds such as metallic [16] and non-metallic [17] pollutants, organic [18–20] and inorganic [21, 22] compounds from aqueous solutions, are more efficient.

The aim of this study is to determine the usage potential of the KOH-activated pine cone biochar in two different application areas. The $CO_2$ retention capacity of the activated biochar product was determined as the first application area in order to reduce $CO_2$ emissions. As a second application area, the effectiveness of activated biochar products in the removal of dyestuff (methyl orange) from aqueous solution was investigated. Methyl orange which is an azo dye usually exists as a sodium salt. It is often used in textile applications because it is sensitive to acids; especially, it has been used to dye wool and silk in an acid bath [23]. Methyl orange's production and use as a dye for textiles may result in its release to the environment through various waste streams. It causes serious problems to the environment because of its high solubility in water and high resistance to biodegradation. Therefore, this dye is removed in a very difficult way from aqueous solution by conventional treatment methods. As targeted in this study, the development of a highly efficient environmentally friendly adsorbent material for reducing $CO_2$ emissions in the atmosphere and removing dyestuffs from the aquatic environment is very important for both the global economy and the environment.

## 2 Materials and methods

### 2.1 Preparation of pine cones

In this study, pine cones (PCs) were used as precursors because of its chemical characteristics similar to those of lignocellulosic biomasses which generally contain 35–55% by weight of cellulose, 20–40% of hemicelluloses, and 10–25% of lignin [24]. The cones were collected from Ankara province in Turkey and air-dried for several days. The dried samples were reduced in size by passing it through a stainless steel blade mill (Waring, USA). Those with dimensions less than 250 μm were used in the pyrolysis process.

### 2.2 Characterization of raw pine cones

#### 2.2.1 Proximate and ultimate analysis

Proximate analysis of the raw material was carried out using an ash furnace (Protherm, PLF120/5). For the volatile matter determination, 1.00 g of sample was placed in a crucible and placed an ash furnace at 950 ± 5 °C temperature and waited 8–10 min. For ash analysis of the samples, 1.00 g of sample was placed in the crucible at 800 °C temperature ash furnace and waited for 60 min. To determine the moisture content of the biomasses, 1.00 g of sample was placed in a crucible and the sample was heated at 70 °C for 24 h. At the end of the processes, the cooled crucibles were weighed and the amount of volatile matter, ash, and moisture were calculated. Ultimate analysis of raw biomasses was performed on the Leco brand CHNS-932 model analyzer. Quantities C, N, H, and S were measured simultaneously.

#### 2.2.2 TG/DTG analysis

The thermal behavior of the raw PC was determined in a thermogravimetric analyzer (TA, DMAQ800). Approximately 10 mg of the sample was placed in the alumina pan and loaded into the device. Experiments were carried out under an inert nitrogen atmosphere using a gas flow rate of 100 mL/min. The temperature was then increased to 800 °C at a heating rate of 20 °C/min and the mass losses of the samples were recorded on the computer as a function of temperature and time.

### 2.3 Pyrolysis processes and preparation of activated pine cone biochar

The pyrolysis process was carried out in two stages. Firstly, to determine the pyrolysis temperature giving the highest surface area, the carbonization of the raw PCs was carried out in an electrically heated fixed bed pyrolysis reactor in a temperature range of 400–700 °C for 1 h, using approximately 40 g of sample. The temperature of reactor which is made from stainless steel was controlled by the thermocouple placed in the reactor. During the process, the inert nitrogen gas flow rate was set to 100 mL/min and the heating rate to 20 °C/min. The reactor temperature was supplied by the heat-couple placed inside the reactor from the top of the furnace. The experimental setup and conditions were described in detail in previous work [25]. The Brunauer-Emmett-Teller (BET) surface areas of biochar products obtained at four different temperatures were measured and the temperature (600 °C) giving the highest surface area (259.74 $m^2$/g) was determined as the carbonization temperature for the raw PCs.

In the second stage of the pyrolysis process, the carbonization and activation processes required to synthesize the PC

biochar with high porosity and high surface area to be used in the experiments were carried out in the cylindrical furnace shown schematically in Fig. 1. For the carbonization process, approximately 550 g of the raw PCs was taken and pyrolyzed in a cylindrical furnace with three homogeneous zones at 600 °C, 10 °C/min heating rate, and 100 mL/min nitrogen flow rate. The carbonized solid product obtained at the end of the process was impregnated using a concentrated KOH solution. The impregnation ratio (weight of carbonized sample/weight of impregnation reagent) was taken as ¼. Activation was carried out by using the impregnated PC biochar, at 10 °C/min heating rate, 100 mL/min nitrogen flow rate, and maximum temperature of 800 °C for 1 h. The activated PC biochar obtained at the end of the process was neutralized using a dilute HCl solution. The active biochar, which was separated by filtration, was washed with silver nitrate solution until no chloride reaction occurred. Finally, the APC biochars were dried at 110 °C for 24 h and were stored in plastic flasks for use in adsorption experiments.

## 2.4 Characterization of activated pine cone biochar

### 2.4.1 Surface analyses

The surface area of the activated pine cone (APC) biochar was obtained from nitrogen adsorption analyses at 77 K by using a Micromeritics/Tristar II Surface area analyzer. Prior to gas adsorption measurement, the sample was degassed at 200 °C under vacuum for 12 h. The adsorption data were obtained in relative pressure. The surface area was calculated from $N_2$ adsorption isotherms by using the BET equation.

The surface functional groups of the APC biochar before and after the adsorption process were examined by FT-IR spectroscopy (Perkin Elmer, Spectrum Two, USA). FT-IR spectra were recorded between 400 and 4000 $cm^{-1}$ by using pellets made with KBr.

To examine the surface properties and microstructure morphology of the biochar samples before and after the adsorption process, topographic images of the sample surface were taken with the Quanta (USA) FEI/Quanta 450 FEG brand SEM device and structural changes were determined.

## 2.5 Determination of the effectiveness of APC biochar in the removal of environmental pollutants

### 2.5.1 $CO_2$ capture

$CO_2$ adsorption capacity of APC biochar was determined using the thermogravimetric analysis method [26]. A Shimadzu brand DTG-60 model simultaneous TG/DTA analyzer was used for measurement. Approximately 10 mg of the sample was placed in the sample holder of the device. The sample was heated at 120 °C for 1 h in a nitrogen atmosphere at a flow rate of 50 mL/min and volatile components were removed from APC biochar's structure. And then the atmosphere of the analyzer was converted to $CO_2$ at the same flow rate and the temperature was reduced to 25 °C. The sample was kept under this condition for 250 min. The amount of $CO_2$ adsorption was calculated from the change of weight in the TG curve. In order to prevent the buoyancy effect, the analyzer was operated in the same test conditions as empty.

### 2.5.2 Adsorption of dyestuff from aqueous solution

Methyl orange (MO) dyestuff was selected as a typical model pollutant due to its potential risk for the environment. It was purchased from Sigma-Aldrich which was of analytical grade and was used without further purification. The detailed information of dyestuff is given in Table 1.

MO was dissolved in distilled water and stored as a stock solution (1000 mg/L). A certain concentration of dye solutions (100–400 mg/L) was prepared by diluting the stock solution. In total, 250 mL of these dye solutions with different initial

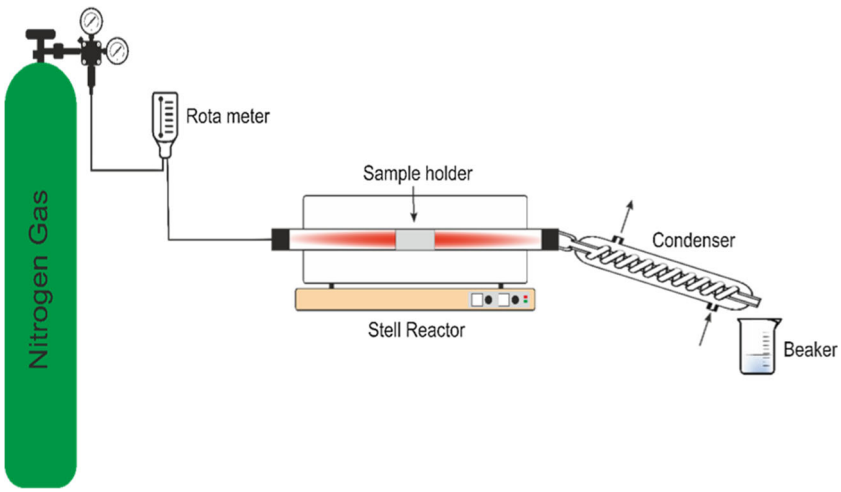


**Fig. 1** Experimental setup of the pyrolysis process (production of activated PC biochar)

**Table 1** Details of the dyestuff used

| | |
|---|---|
| **Dyestuff** | Acid Orange 52 |
| **IUPAC Name** | Sodium;4-[[4-(dimethylamino) phenyl]diazenyl] benzenesulfonate |
| **Commercial Name** | Methyl Orange |
| **C.I. Number** | 13025 |
| **CAS Number** | 547-58-0 |
| **Appearance** | Orange powder |
| **Empirical Formula** | $C_{14}H_{14}N_3NaO_3S$ |
| **Molecular Weight** | 327.34 g/mol |
| **3D Molecular Structure** | 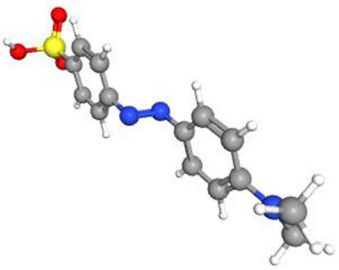 |
| **Chemical Structure** | 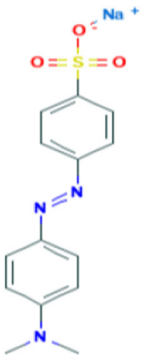 |
| $\lambda_{max}$ | 464 nm |

concentrations was put in a series of 500-mL Erlenmeyer flasks. Parameters affecting the adsorption process such as pH (2–10), adsorbent dosage (0.1–0.8 g/L), and temperature (25–45 °C) were studied in a batch system. The solution pH was adjusted using dilute HCl (0.1 M) and NaOH (0.1 M). The dye adsorption process was carried out in an isothermal water bath shaker with a rotation speed of 150 rpm. The experiment was carried out for 250 min to ensure that the equilibrium was reached. The samples were collected at predetermined time intervals and adsorbent separated from the samples by filtering in order to minimize the interference of the carbon fines. For this purpose, a Whatman filter paper (size 41) was used. The residual dye concentration in samples was measured using a UV-Visible spectrophotometer

(DR2400, Hach Company, USA). Based on the acquired values, the amount of dye adsorbed per unit mass of the adsorbent ($q_e$) was calculated according to Eq. (1) and the adsorption yield was calculated by using Eq. (2) [27].

$$qe = (C0-Ce)\ x\frac{V}{m} \quad (1)$$

$$\text{Dye removal}\ (\%) = \frac{C_0-C_e}{C_0} \times 100 \quad (2)$$

where $q_e$ is the amount of adsorbed dye per gram of adsorbent (mg/g), $C_o$ and $C_e$ are the initial and final dye concentrations in solution phase, respectively (mg/L), $V$ is the volume of dye solution (L), and $m$ is the weight of adsorbent (g). In order to ensure the reproducibility of the results, all the adsorption experiments were performed in triplicate and the average values were used in data analysis. Relative standard deviations were found to be within ± 2%.

## 3 Results and discussion

### 3.1 Characterization of raw PC

The physicochemical properties of the raw pine cone are presented in Table 2. PC had a high content of volatile substances (72.0%). The high volatiles in the pyrolysis process drift away from the environment due to the effect of temperature and the fixed carbon remains, the main component of the biochar. However, the amount of ash contained in the biomass is also very important in the pyrolysis process. High ash content is important as it causes contamination and aggregation in the reactor. At the same time, it affects the pyrolysis quality and causes an increase in operating costs. The ash value of pine cone (3.20%) presented in this study was high compared with that of other biomass species reported in the literature [28]. Although the main element of biochar is carbon (C), it also contains hydrogen (H), oxygen (O), small amount of nitrogen (N), and sulfur (S). The elemental composition of biochars varies depending on the type of raw biomass and pyrolysis conditions [29]. According to elemental analysis results, pine cone had a low sulfur content (0.025%). S content is critical due to environmental issues such as $SO_2$ gas emissions and acid rains. Also, a low nitrogen content in biomass means less toxic nitrogen oxide emissions during combustion. The nitrogen and sulfur content of the PC used in this study was low compared with that in other biomass types reported in the literature [28].

Figure 2 presents the thermogravimetric (TG) and derivative thermogravimetric (DTG) curves of PC under inert nitrogen atmosphere for the final temperature of 800 °C and a heating rate of 20 °C/min. When TG and DTG curves were analyzed, it was seen that decomposition of PC took place in three steps. The first decay began at 27 °C and ended at 113 °C. At this step, the moisture and the low molecular weight substances were removed from the surface. The main decomposition of PC started at 205 °C and ended at 468 °C. At this step, the mass loss was high and this showed that hemicellulose, cellulose, and lignin were decomposed. Lignocellulosic biomass consists of hemicellulose, cellulose, and lignin. In the literature, the decomposition temperature ranges of hemicellulose, cellulose, and lignin are reported as 210–325, 310–400, and 160–900 °C, respectively. When the thermogravimetric analysis curves of the PC used in this study were compared with other lignocellulosic biomass species, it was found to be compatible with the literature [28, 30].

### 3.2 Structural characterization of activated PC biochar

In order to obtain information about the surface properties of activated PC biochar, BET surface area and micropore volume values were determined and presented in Table 3. The BET surface area and pore volume values of the activated biochar product were measured as 1714.5 $m^2/g$ and 0.684 $cm^3/g$, respectively. Biochars with low surface area are undesirable especially for adsorption studies [31]. It is known that adsorbents with high surface area and small particle size are more effective in the adsorption process. However, it is a known fact that significant improvements have been achieved thanks to chemical activations in the surface area and pore volume, which are important parameters for biochar applications. Chemical activation can not only increase the porosity of the biochar but also affect the chemical properties of the surface (surface functional groups, hydrophobicity, and polarity) [32]. In the literature, there are many biochar products activated with different chemical reagents and used for different applications. For example, Li et al. (2015) measured the surface area value of the biochar they obtained from rice husk at 520

**Table 2** Proximate and ultimate analysis of PC

| Pine cone | |
|---|---|
| Proximate analysis | |
| Volatile matter | 72.0 |
| Ash | 3.20 |
| Fixed carbon[a] | 24.8 |
| Ultimate analysis | |
| C | 44.75 |
| H | 5.37 |
| N | 0.59 |
| S | 0.025 |
| O[a] | 49.27 |
| Higher heating value (MJ/kg) | 14.09 |

[a] Calculated by difference

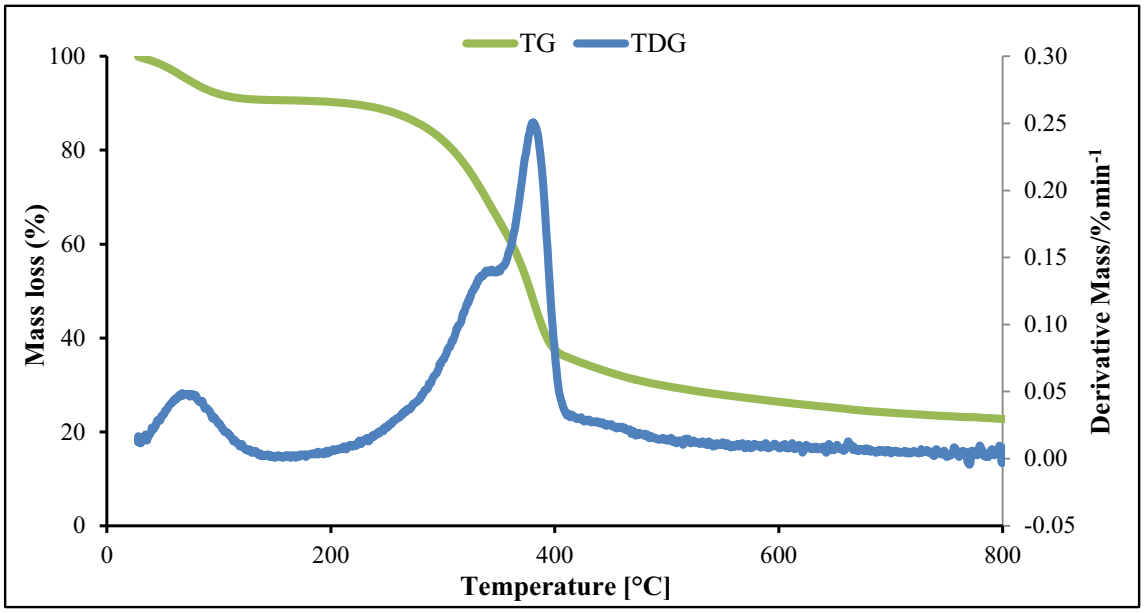


**Fig. 2** TG and DTG curves of raw PC at 20 °C/min

°C as 2695 $m^2/g$ [33]. Biswas et al. (2020) determined the surface area value of the biochar which is activated with $H_3PO_4$ obtained from the pine cone as 171.85 $m^2/g$ [34]. In this study, it was seen that the surface area value of the biochar obtained from the PC and activated with KOH was quite high compared with many studies in the literature. While the surface area of the non-activated PC biochar was 259.74 $m^2/g$, this value increased to 1714.5 $m^2/g$ as a result of the chemical activation process. This result suggests that activated PC biochar may be a good carbon-based material to be used as an adsorbent for removing environmental pollutants.

### 3.3 $CO_2$ adsorption capacity of activated PC biochar

Due to modern life needs such as electricity, transportation, and industrialization, consumption of fossil fuels inevitably continues. As a result of these activities, greenhouse gases that cause global warming are released into the environment. Among these emissions, $CO_2$ has a significant impact and share. According to the Intergovernmental Panel on Climate Change (IPCC) special report of global warming (2018), it is stated that to limit global warming to just under 2 °C, $CO_2$ emissions should be reduced by 25% until 2030 and reduced by 100% until 2070 [35]. $CO_2$ should be removed from the atmosphere. For this purpose, various technologies related to carbon capture storage are being developed to limit the effects of emissions [36–38]. One of the most convenient methods for capturing $CO_2$ is undoubtedly adsorption. In this study, $CO_2$ adsorption performance test of the activated PC biochar sample was performed in TGA. The change in TG curve over time is shown in Fig. 3. As can be seen from Fig. 3, the maximum $CO_2$ adsorption capacity of activated PC biochar product was 160 mg/g (3.64 mmol/g) at 25 °C. Experimental results indicated that $CO_2$ adsorption was completed within 180 min. There are some studies in the literature on $CO_2$ storage onto activated biochar products at different temperatures. Ambient temperature is the most important factor affecting adsorption capacity values. Mostly, the increase in ambient temperature leads to a significant decrease in the adsorbed values of $CO_2$ [39]. For example, $CO_2$ absorptivity of $K_2CO_3$-activated cashew nutshell carbon is found to be between 4.16 and 6.22 mmol/g at atmospheric

**Table 3** Surface characteristics of PC biochar

| Samples | Pyrolysis conditions | Activation conditions | $S_{BET}$ ($m^2/g$) | Pore volume ($cm^3/g$) | Reference |
|---|---|---|---|---|---|
| PC biochar | 600 °C, 1 h | No activation | 259.74 | - | [25] |
| Activated PC biochar | 600 °C, 1 h | KOH impregnation ratio ¼<br>800 °C<br>1 h | 1714.5 | 0.684 | This study |

**Table 4** Comparison of $CO_2$ adsorption capacities of activated biochars produced from different biomasses

| Biomass type | Activation method | $S_{BET}$ ($m^2$/g) | $CO_2$ capture (mmol/g) | Reference |
|---|---|---|---|---|
| Pine cone | KOH | 1714.5 | 3.64 | This study |
| Rice husk | HF | 451 | 1.80 | [41] |
| Vine shoots | KOH | 1439 | 1.98 | [42] |
| Camellia japonica | KOH | 3537 | 2.80 | [43] |
| Rice husk | KOH | 2695 | 3.71 | [44] |
| Coconut shell | $H_3PO_4$ | 1322 | 3.73 | [45] |
| Pomegranate peel | KOH | 585 | 4.00 | [46] |
| Pine nutshell | KOH | 1486 | 5.00 | [47] |

pressure and 0 °C [40]. On the other hand, the adsorption capacity values given in Table 4 are the values obtained at 25 °C in the literature. The results show that $CO_2$ uptake at 0 °C was slightly better than 25 °C.

At the same time, as seen from Table 4, an extremely high increase in specific surface area and $CO_2$ adsorption was observed for the samples modified with KOH compared with acid activation. In acid activation, especially the surface area and adsorption capacity of the HF-activated biochar product was quite low compared with the $H_3PO_4$-activated biochar product. Therefore, it can be said that the biochar products activated with KOH are more useful in $CO_2$ capture applications. Especially the $CO_2$ adsorption capacity of the active biochar prepared from pine cone within the scope of the study was higher than many other biochar products reported in the literature [7, 32]. Thanks to the KOH activation, the surface area and adsorption capacity of the biochar have been increased, making it comparable to the adsorption capacities of other biochars reported in the literature. The experimental result indicated that this material can be used in $CO_2$ capture applications. Based on the results, it can be concluded that it is absolutely necessary to activate the biochar in order to keep a higher amount of $CO_2$.

## 3.4 Adsorption of methyl orange onto activated PC biochar

The adsorption capacity of the produced APC biochar was also tested for the removal of MO from aqueous solution. The effects of different adsorption parameters such as pH of solution, initial concentration of dye solution, contact time, adsorbent dosage, and temperature on the adsorption of MO onto APC biochar were investigated and optimized in batch experimental system. The equilibrium of adsorption was modeled using the Langmuir and Freundlich isotherm models. Pseudo-first-order and pseudo-second-order kinetic models were used to test the adsorption data. Thermodynamic parameters such as the Gibbs free energy, enthalpy, and entropy were determined.

### 3.4.1 Effect of initial solution pH

The basic mechanism in the adsorption process depends on the interest of the substance to be adsorbed on the solid surface used as adsorbent. Therefore, not only the surface area of the adsorbent but also the chemical structure of this porous material and ambient chemistry are of great importance. It is known that

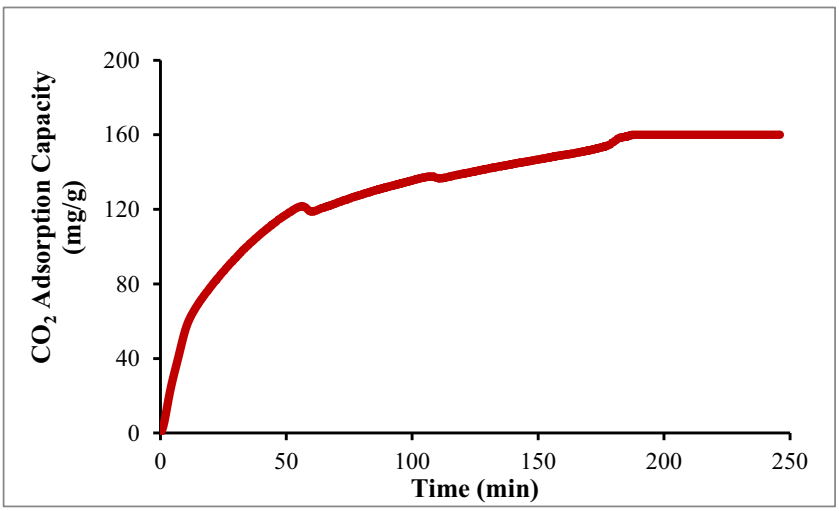


**Fig. 3** $CO_2$ adsorption capacity of the activated PC biochar

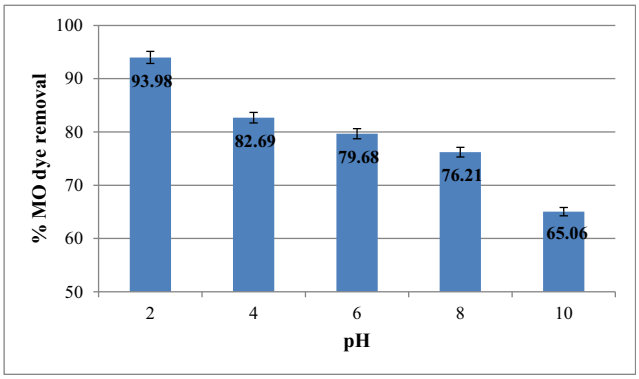


**Fig. 4** Percentage MO dye removal at different pH

the pH value of the solution has an important role in the adsorption process especially in the surface charge of adsorbent, electrostatic interaction, hydrogen bond formation, electron exchange, and π-π dispersion interactions in solution [48]. Also, since hydronium and hydroxide ions are strongly adsorbed in the aqueous medium, the adsorption of other ions is affected by the pH of the solution. In this study, the effect of pH was determined in the pH range from 2 to 10 at a fixed initial concentration (100 mg/L), temperature (25 °C), adsorbent dosage (0.8 g/L), and time (250 min). The influence of pH on the adsorption of MO onto APC biochar is illustrated in Fig. 4. It was observed that the percentage removal of MO decreased as pH increased. The maximum amount of MO (93.98%) adsorbed was obtained at pH of 2. While the solution pH increased, adsorption capacity value also decreased from 109.5 to 81.3 mg/g. This result could be attributed to the fact that the MO is an anionic dye. At low pH values, the adsorbent surface becomes positively charged and therefore, electrostatic attraction between the adsorbent surface and negatively charged dye molecule increases. As a result, a greater amount of dye is adsorbed [49, 50]. In other words, at high pH values, excess $OH^-$ ions in the solution compete with the anionic groups of the dye molecule for attaching to the adsorption sites on the adsorbent surface which leads to a decrease in adsorption yield [8, 51]. In addition, activation of the PC biochar with KOH caused hydroxyl groups to exist on the surface of the adsorbent. The adsorption of MO onto activated PC biochar may have occurred by the displacement of the anionic group of the MO with the $OH^-$ group of the biochar [52].

### 3.4.2 Effect of temperature

Temperature is another important parameter affecting adsorption. It is a factor that determines not only the adsorption efficiency but also the type of process, whether it is physical or chemical. The effect of temperature was investigated in the temperature range from 25 to 45 °C at a fixed initial concentration of 100 mg/L, pH of 2, adsorbent dosage of 0.8 g/L, and time of 250 min. The adsorption yields obtained from MO removal from aqueous solutions at three different temperatures are given in Fig. 5. The decrease in adsorption efficiency at high temperature indicated that the adsorption process was more favorable at lower temperatures. The results showed that when using APC biochar, the adsorption efficiency decreased from 93.98 to 80.99% with the increasing temperature so that the process was physical. This is because it is known that the low-temperature range is sufficient in the physical adsorption due to van der Waals forces, which in turn leads to a decrease in the adsorption efficiency with increasing temperature [53]. In addition, the decrease in the adsorption capacity with the increasing temperature showed that the adsorption process was exothermic.

### 3.4.3 Effect of initial dye concentration and adsorbent dosage

In order for the adsorption process to take place, some conditions must occur. Dissolved substances to be kept on the

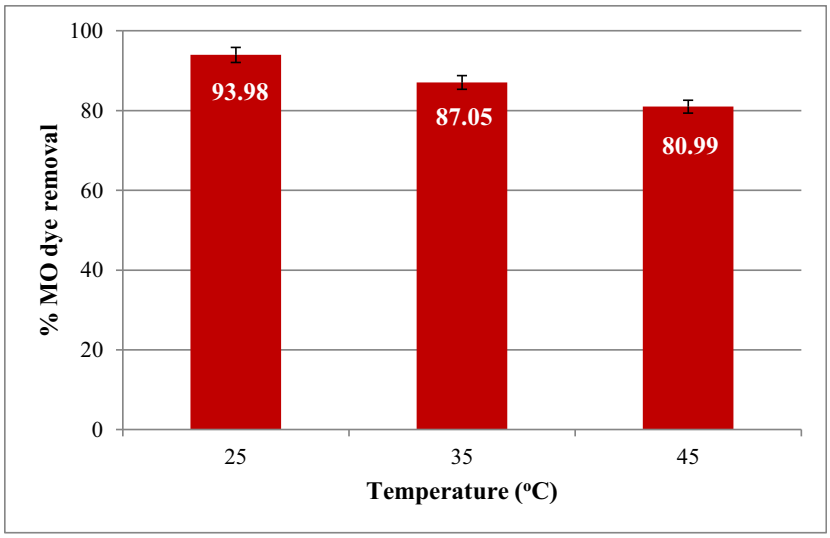


**Fig. 5** Percentage MO dye removal at different temperatures

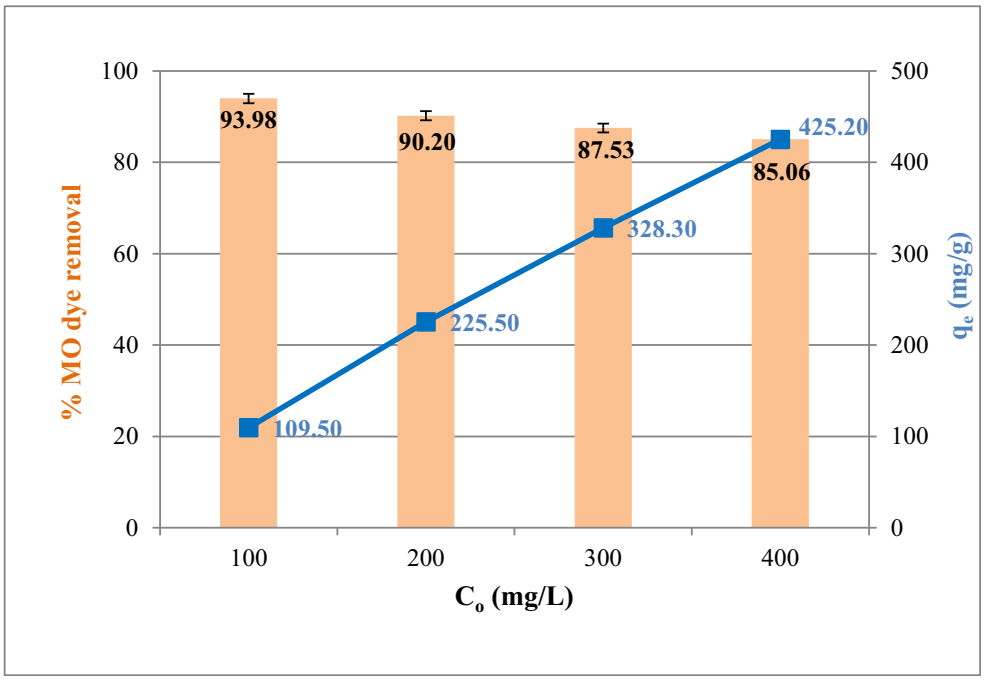


**Fig. 6** Adsorption efficiency and adsorption capacity values for different initial dye concentrations (pH = 2, T = 25 °C, adsorbent dosage = 0.8 g/L)

adsorbent surface must first pass through the solvent liquid film surrounding the mass. This transition is called "film diffusion." The substances coming to the adsorbent surface must complete a transition called "pore diffusion" in order to enter the inner part of the pores. Binding of the dissolved substance that passes these two stages on the adsorbent substance is the last process. At this point, the initial concentration of the substance to be adsorbed on the solid surface is very important because the most important driving force between the liquid and solid phase is undoubtedly the initial concentration. The effects of different initial MO concentrations on adsorption yield and adsorption capacity values are shown in Fig. 6. The experimental results showed that by changing the initial concentration for MO dye at the range of 100–400 mg/L, the adsorption efficiency decreased, whereas the adsorption capacity values increased. Experimental results showed that all dye molecules in the solution phase, particularly at low concentrations, interacted with the binding sites of the adsorbent and resulting in high removal efficiencies. However, it should be noted that all adsorbents saturated at a given concentration have a limited number of binding sites. Therefore, the possibility of attachment of the dye molecules on the adsorbent surface was weakened with increasing initial dye concentration and the removal efficiencies also decreased. On the other

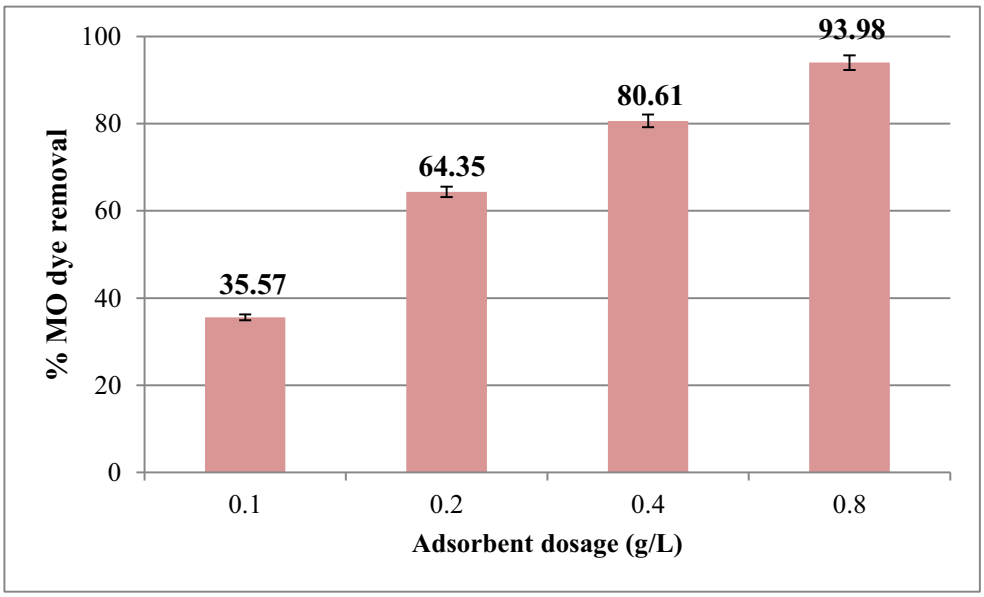


**Fig. 7** Percentage MO dye removal at different adsorbent dosage (pH = 2, T = 25 °C, $C_o$ = 100 mg/L)

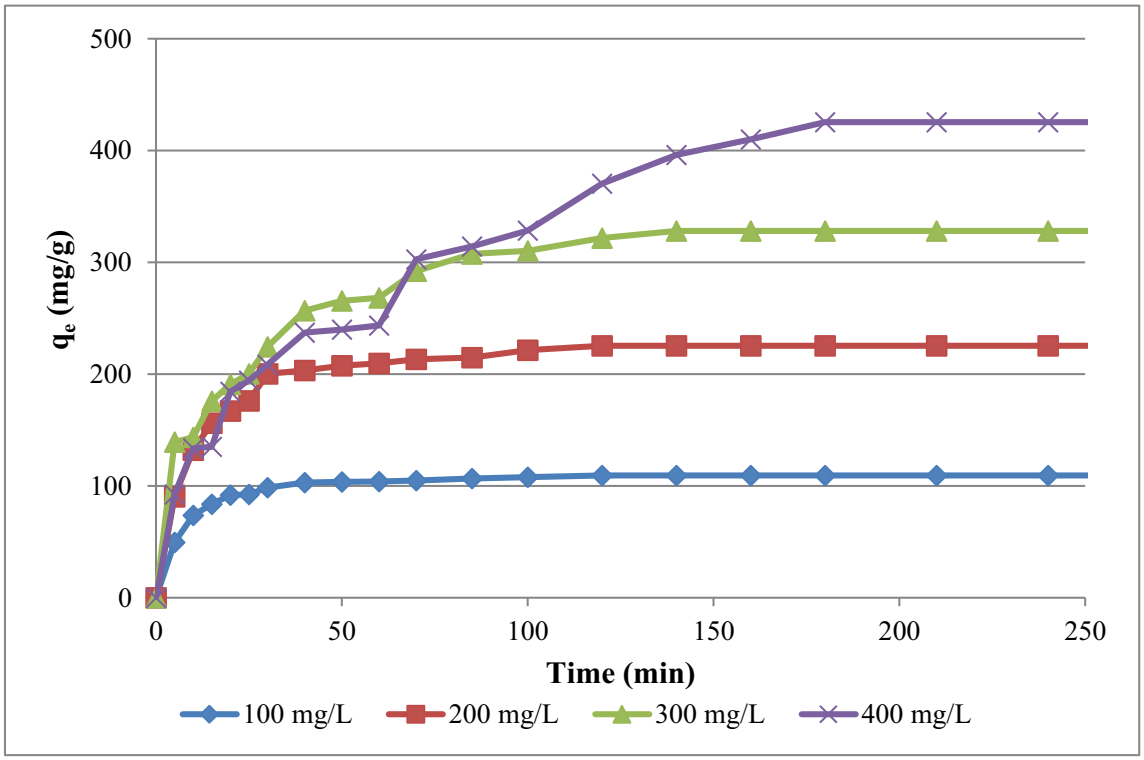


**Fig. 8** Effect of contact time and initial concentration on the adsorption of MO dye onto APC biochar (pH = 2, T = 25 °C, adsorbent dosage = 0.8 mg/L)

hand, the increased initial concentration, which is the important driving force for the mass transfer between the aqueous solution and the solid phase, caused an increase in the equilibrium adsorption capacity ($q_e$) [54]. An increase in the initial concentration of MO solution from 100 to 400 mg/L resulted in an increase of the adsorption capacity of APC biochar of nearly 290% (from 109.5 to 425.2 mg/g).

Since the adsorption process is an event occurring on the surface of the material, the efficiency of the adsorption is proportional to the specific surface area of the adsorbent. That is, it is desirable that the adsorbent has a large surface area, pore volume, and a certain pore size distribution. However, the amount of adsorbent to be used in the adsorption process is also very important. In this study, the effect of adsorbent dosage was investigated by varying the adsorbent amounts from 0.1 to 0.8 g/L and the experimental results are shown in Fig. 7. It was observed that the removal efficiency of MO increased from 35.57 to 93.98% when the adsorbent dosage increased. This result could be attributed to the availability of more and more active binding sites with the increasing dosage of the adsorbent [55]. Therefore, increasing the adsorbent dosage was another factor that positively affected the adsorption process due to a large surface area allowed.

### 3.4.4 Effect of contact time

In order to examine the effect of contact time on the adsorption process and to determine the optimum contact times at which the maximum dye removal efficiency was achieved at different initial concentrations, dye solutions of different concentrations were contacted with a certain amount of APC biochar. Figure 8 shows the effect of contact time and initial MO dye concentrations at 25 °C on the amount of MO dye adsorbed per gram of APC biochar. It was observed that the adsorption rate was quite high for the first 30 min in all concentrations studied. Then, the adsorption process continued at a slow rate and finally attained saturation at different time intervals due to different initial concentrations of dye solutions. The adsorption process was completed within approximately 85–180 min for initial concentrations of 100–400 mg/L. When the equilibrium was reached, there was no change in the adsorption capacities. The higher adsorption rate at the initial period could

**Table 5** Maximum adsorption capacity values for removal of MO dye using different adsorbents (initial MO concentration of 100 mg/L)

| Adsorbent | $q_e$ (mg/g) | Reference |
|---|---|---|
| Chitosan/rectorite/carbon nanotubes composite | 50.8 | [56] |
| Fly ash modified by $Ca(OH)_2/Na_2FeO_4$ | 67.9 | [57] |
| Commercially activated carbon | 77.0 | [58] |
| Pine sawdust–activated carbon | 91.9 | [52] |
| Granular-activated carbon | 46.1 | [59] |
| Activated PC biochar | 109.5 | This study |

**Table 6** Freundlich and Langmuir isotherm constants for the adsorption of MO onto APC biochar

| Adsorbent type | Isotherm model | Parameters | Temperature (°C) | | |
|---|---|---|---|---|---|
| | | | 25 | 35 | 45 |
| APC biochar | Langmuir | $q_{max}$ (mg/g) | 80.37 | 69.93 | 57.88 |
| | | $K_L$ (L/mg) | 0.261 | 0.1874 | 0.1138 |
| | | $R^2$ | 0.9202 | 0.9193 | 0.8970 |
| | Freundlich | $K_f$ [mg/g (L/mg)$^{1/n}$] | 20.18 | 19.15 | 20.38 |
| | | $n$ | 0.421 | 0.459 | 0.417 |
| | | $R^2$ | 0.9821 | 0.9880 | 0.9919 |

be attributed to the availability of more vacant sites at the surface of the adsorbent at the beginning [8].

It is concluded that APC biochar was a superior adsorbent for MO removal because the value of the adsorption capacity was quite high in comparison with that in several other reported adsorbents in the literature (Table 5).

### 3.4.5 Adsorption isotherm models

Adsorption isotherms are important to understand how adsorbed molecules distribute between the solid and liquid phases when the equilibrium is reached in the adsorption process. The adsorption isotherm study was carried out on two well-known isotherms to test the adsorption data; they are the Langmuir and Freundlich adsorption models. The Langmuir isotherm, which is considered to occur on a homogeneous surface, is based on the following assumptions: The adsorbent surface has a constant number of active sites with the same energy and the adsorption energy is constant. Adsorption occurs in a monolayer and maximum adsorption occurs when the molecules attached to the adsorbent surface form a saturated layer. This is the simplest theoretical model for the adsorption process, which is expressed by Eq. (3). The Freundlich model assumes that the adsorption process takes place on multilayered heterogeneous surfaces and is expressed by the formula in Eq. (4).

$$\frac{C_e}{q_e} = \frac{C_e}{q_{max}} + \left(\frac{1}{q_{max} K_L}\right) \tag{3}$$

$$\ln q_e = \ln K_f + \frac{1}{n} \ln C_e \tag{4}$$

where $C_e$ is the equilibrium concentration of dye in the bulk solution (mg/L), $q_e$ is the amount of dye adsorbed per unit mass of adsorbent (mg/g), $q_{max}$ is the maximum adsorption capacity (mg/g), $K_L$ is the constant related to the free energy of adsorption (L/mg), $K_f$ is a Freundlich constant indicative of the relative adsorption capacity of the adsorbent [mg/g (L/mg)1/$n$], and 1/$n$ is the heterogeneity factor which is the constant characteristics of the system [60]. With the application of the results obtained experimentally to the Langmuir and Freundlich isotherm models, the linear isotherm graphs $C_e/q_e$ versus $C_e$ and $\ln q_e$ versus $\ln C_e$ were drawn. The model parameters calculated from these graphs are given in Table 6.

As it was seen from Table 6 that the correlation coefficients ($R^2$ values) for Freundlich isotherm were higher than that of Langmuir isotherm and they were very close to 1. Therefore, the best fit was achieved by the Freundlich isotherm equation. Fit of this equation reflected heterogeneous surface or in other words indicated that multilayer sorption of the surface. On the other hand, the adsorption process was a physical process because of the fact that 1/$n$ values are higher than 1. This result was similar to those obtained by studies on the effect of temperature on the adsorption process in order to characterize the adsorption model. As a result, this adsorption isotherm provided some insight into the adsorption mechanism and the surface characteristics of the adsorbent. A similar observation is reported in the literature [51].

**Table 7** Rate constants of pseudo-first-order and pseudo-second-order models with correlation coefficients

| Adsorbent type | Initial concentration(mg/L) | $q_e$ (exp)(mg/g) | Pseudo first order | | | Pseudo second order | | |
|---|---|---|---|---|---|---|---|---|
| | | | $q_e$ (cal)(mg/g) | $K_1$(1/min) | $R^2$ | $q_e$ (cal)(mg/g) | $K_2$(g/mg.min) | $R^2$ |
| APC biochar | 100 | 109.5 | 49.52 | 0.1570 | 0.904 | 112.36 | $2.02 \times 10^{-3}$ | 0.999 |
| | 200 | 225.5 | 244.74 | 0.1247 | 0.973 | 232.56 | $6.68 \times 10^{-4}$ | 0.998 |
| | 300 | 328.3 | 257.16 | 0.0125 | 0.981 | 357.14 | $2.05 \times 10^{-4}$ | 0.994 |
| | 400 | 425.2 | 401.42 | 0.0077 | 0.954 | 476.19 | $6.14x \times 10^{-5}$ | 0.978 |

**Table 8** Thermodynamic parameters of MO adsorption onto APC biochar at different temperatures

| Adsorbent type | Temperature (°C) | $\Delta G^o$ (kJ/mol) | $\Delta H^o$ (kJ/mol) | $\Delta S^o$ (kJ/mol.K) |
|---|---|---|---|---|
| APC biochar | 25 | − 4.841 | - 78.92 | 41.08 |
| | 35 | − 4.788 | | |
| | 45 | − 4.638 | | |

### 3.4.6 Adsorption kinetics and thermodynamic study

Adsorption kinetics were investigated in order to examine the adsorption mechanism, determine the adsorption rate, and calculate the maximum adsorption capacity of the APC biochar for MO adsorption. Adsorption data were tested using two different kinetic models: pseudo-first-order and pseudo-second-order kinetic models. The linear forms of pseudo-first-order and pseudo-second-order rate equations are presented in Eqs. (5) and (6), respectively.

$$\log(q_e - q_t) = \log(q_e) - \frac{k_1}{2,303}t \quad (5)$$

$$\frac{t}{q_t} = \frac{1}{k_2 q_e^2} + \frac{t}{q_e} \quad (6)$$

where $q_t$ and $q_e$ denote the sorption capacity (mg/g) at a given time and at equilibrium, respectively, $k_1$ is the pseudo-first-order rate constant (1/min), and $k_2$ is the pseudo-second-order rate constant (g/mg·min) [61]. With the application of the results obtained experimentally to the pseudo-first- and second-order kinetic models, the linear graphs $\log(q_e\text{-}q_t)$ versus $t$ and $t/q_t$ versus $t$ were drawn. The rate parameters were calculated from the slope and intercept of these graphs. The values of kinetic parameters (the rate constants of the two models with the correlation coefficients) of the linear form of both rate equations are presented in Table 7.

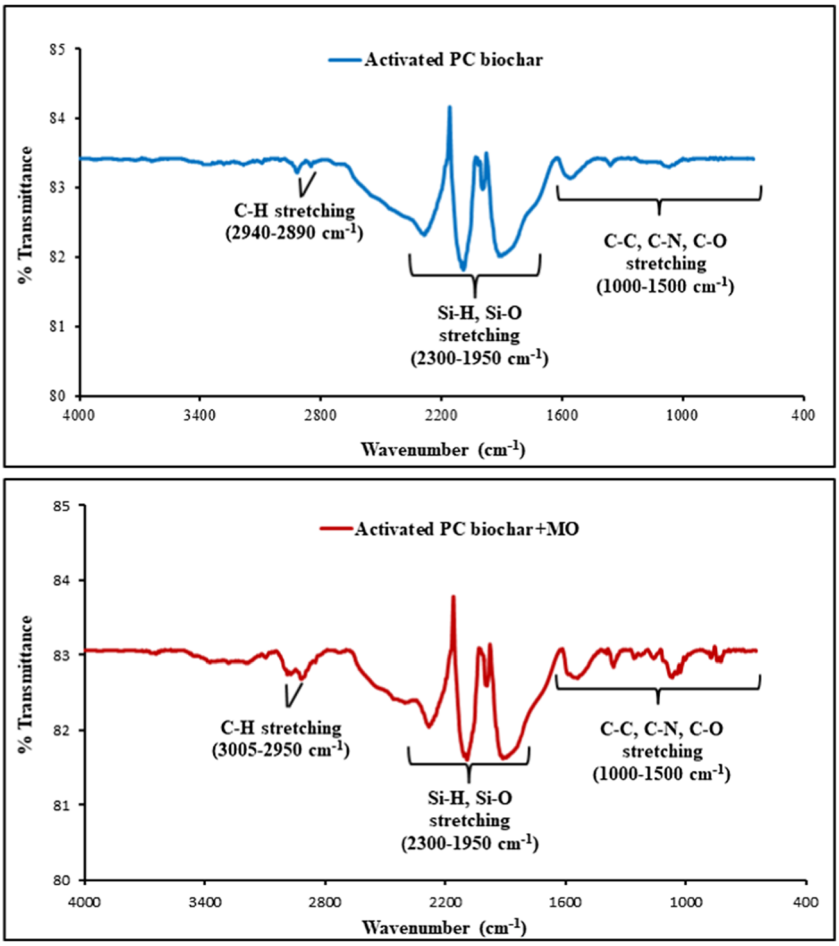


**Fig. 9** FT-IR spectra of the activated PC biochar before and after MO adsorption

The pseudo-second-order kinetic model fit the adsorption data well when compared with the pseudo-first-order kinetic model because of the correlation coefficients between 0.978 and 0.999 were high and the calculated equilibrium adsorption capacity values were in agreement with the experimental equilibrium adsorption capacity values shown in Table 7. Also, it was clear that as the initial concentration of the dye solution increased, the value of the rate constants ($K_1$ and $K_2$) decreased. This result showed that as the initial concentration increased, great adsorption occurred but it was slower than lower concentrations; i.e., the adsorption took place slowly. A similar observation is reported in the literature [52, 62].

Enthalpy ($\Delta H^o$), entropy ($\Delta S^o$), and free energy changes ($\Delta G^o$) should also be examined to get information about the nature of adsorption. These thermodynamic parameters were calculated using the following Eqs. (7–9):

$$\mathrm{Kc} = \frac{C_{\mathrm{ads}}}{C_{\mathrm{e}}} \tag{7}$$

$$\Delta G = -RT\ln\mathrm{Kc} \tag{8}$$

$$\ln\mathrm{Kc} = \frac{\Delta S}{R} - \frac{\Delta H}{RT} \tag{9}$$

where $K_c$ is the equilibrium constant (L/mg), $R$ (8.314 J/mol K) is the universal gas constant, and $T$ (K) is the absolute solution temperature. The values of $\Delta H^o$ and $\Delta S^o$ were determined from the slope and intercept of the Van't Hoff graph obtained by the plotting $\ln K_c$ versus $1/T$ [50]. The calculated thermodynamic parameters are given in Table 8. It was seen from this table that the negative value of $\Delta G^o$ indicated the spontaneous nature and feasibility of the adsorption process. The negative value of $\Delta H^o$ showed the exothermic nature of the process. The positive value of $\Delta S^o$ indicated an increase in the randomness at the solid/solution interface during the adsorption process.

### 3.5 Surface characteristics of activated PC biochar (before and after MO adsorption)

The FT-IR spectra of activated PC biochar samples before and after MO adsorption were recorded between 400 and 4000 $cm^{-1}$ and are shown in Fig. 9. In the obtained spectra, the structures of the samples were defined with the help of the peaks given by the surface functional groups. When the FT-IR spectrum before the adsorption was examined, C–H stress vibrations due to aliphatic hydrocarbons were observed in the 2940–2890 $cm^{-1}$ wave number. The band observed at 3005 $cm^{-1}$ after adsorption could be caused by the C–H tensile band in the aromatic ring in the structure of the MO [63, 64]. Some functional groups have emerged after adsorption. These groups were the stress peaks corresponding to the wavenumber of 1269, 1212, and 1086 $cm^{-1}$. Especially, these bands were sharp and more distinct after adsorption. Therefore, the peaks in the range of approximately 1000–1500 $cm^{-1}$ wave number proved that the MO was adsorbed [63]. Sharp and intense bands seen before and after adsorption could be attributed to Si–O and Si–H stress vibrations [65–68]. As a result,

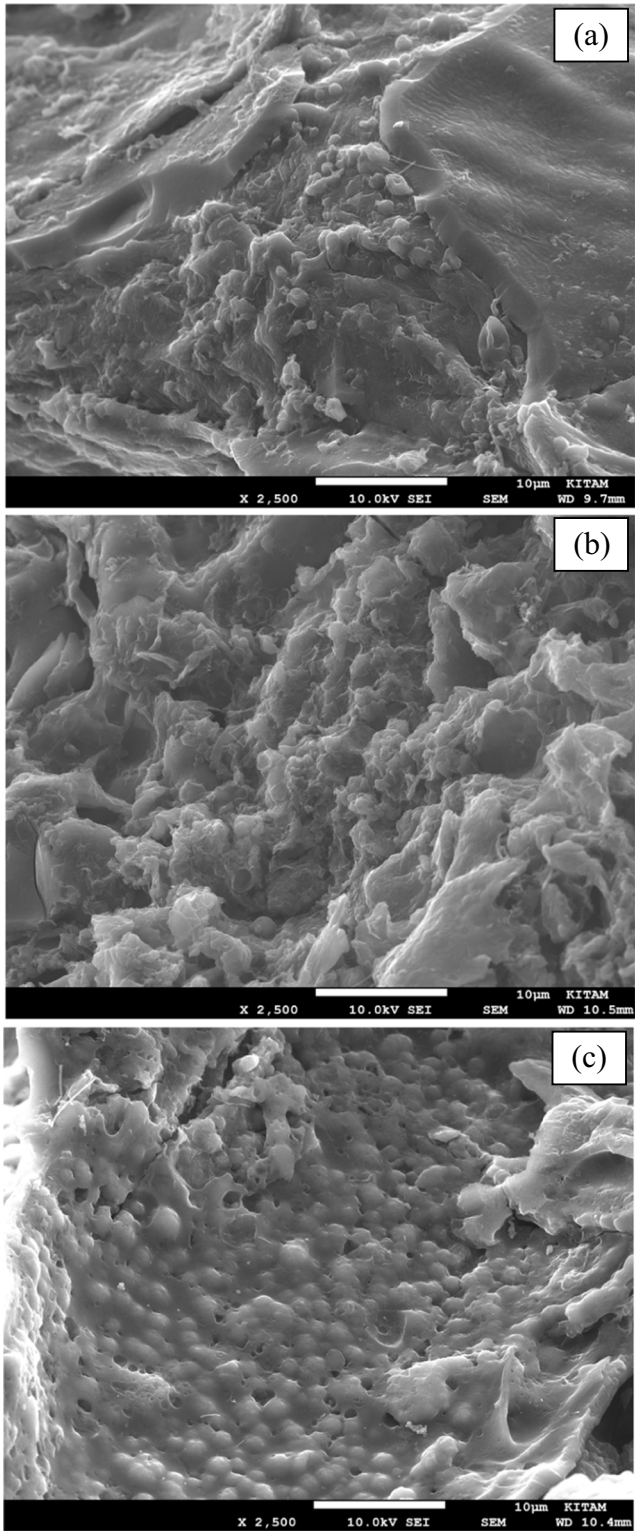


**Fig. 10** SEM images of the PC biochar; **a** No activation, **b** activation with KOH (before adsorption process), **c** APC biochar after adsorption process

FT-IR spectra recorded before and after adsorption showed the presence of various functional groups in the structure due to the adsorption of MO.

Figure 10 shows the SEM images of PC biochar samples (with and without activation). The KOH activation was effective in creating well-developed pores on the surface of the biochar. Pore volume and surface area increased due to the reaction between carbon in the structure of the biochar, and KOH solution and also the formation of new functional groups [69]. Especially with the formation of new pores as a result of chemical activation, the surface area increased from 259.74 to 1,714.5 $m^2/g$. The image in Fig. 10b clearly showed the change in surface morphology after the chemical activation. Surface images taken after adsorption process (Fig. 10c) clearly showed that the surface of the APC changed considerably after the treatment and that MO dye molecules, which were desired to be removed from the aqueous solution in operation, were held by the pores significantly.

## 4 Conclusions

In this study, carbonaceous material with high surface area was produced by using the chemical activation method. A significant increase in surface area (from 259.74 to 1714.5 $m^2/g$) was achieved with KOH activation. Obtained APC biochar was used as adsorbent for $CO_2$ storage and MO removal from aqueous solution. High $CO_2$ uptake (160 mg/g) and high MO removal (93.98%) obtained were clearly shown the importance of surface properties of carbonaceous materials on the adsorption process. The adsorption kinetics and isotherm studies for MO removal indicated the effectiveness and applicability of the APC biochar under various process conditions. Thermodynamic parameters indicated the spontaneous, exothermic, and the increased randomness nature of MO adsorption. Experimental results showed that APC biochar is a highly effective and potential adsorbent that could be used in both water treatment and reduction of $CO_2$ emission due to its high removal efficiency for both MO and $CO_2$. In addition, given that biochars can be regenerated or recycled by thermal, steam, and chemical methods, it is an undeniable fact that these materials are cost-effective.

**Acknowledgments** The authors would like to thank the Hitit University and Ondokuz Mayıs University for their support and also would like to thank Assoc. Prof. Dr. Yunus Onal for his support in the preparation of activated biochar product.

### Compliance with ethical standards

**Conflict of interest** The authors declare that there is no conflict of interest.

## References

1. Kambo HS, Dutta A (2015) A comparative review of biochar and hydrochar in terms of production, physico-chemical properties and applications. Renew Sust Energ Rev 45:359–378. https://doi.org/10.1016/j.rser.2015.01.050
2. Zhang Z, Zhu Z, Shen B, Liu L (2019) Insights into biochar and hydrochar production and applications: a review. Energy 171:581–598. https://doi.org/10.1016/j.energy.2019.01.035
3. Wang J, Wang S (2019) Preparation, modification and environmental application of biochar: a review. J Clean Prod 227:1002–1022. https://doi.org/10.1016/j.jclepro.2019.04.282
4. Cha JS, Park SH, Jung SC, Ryu C, Jeon JK, Shin MC, Park YK (2016) Production and utilization of biochar: a review. J Ind Eng Chem 40:1–15
5. Sun Y, Zhang Z, Sun Y, et al (2020) One-pot pyrolysis route to Fe-N-Doped carbon nanosheets with outstanding electrochemical performance as cathode materials for microbial fuel cell. Int J Agric & Biol Eng doi: 10.25165/j.ijabe.20201306.5765
6. Sasi Kumar N, Grekov D, Pre P, Alappat BJ (2020) Microwave mode of heating in the preparation of porous carbon materials for adsorption and energy storage applications- an overview. Renew Sust Energ Rev 124:109743
7. Creamer AE, Gao B, Zhang M (2014) Carbon dioxide capture using biochar produced from sugarcane bagasse and hickory wood. Chem Eng J 249:174–179. https://doi.org/10.1016/j.cej.2014.03.105
8. Ojo T, Ojedokun A, Bello O (2019) Functionalization of powdered walnut shell with orthophosphoric acid for congo red dye removal. Part Sci Technol 37(1):74–85. https://doi.org/10.1080/02726351.2017.1340914
9. Aygün A, Yenisoy-Karakaş S, Duman I (2003) Production of granular activated carbon from fruit stones and nutshells and evaluation of their physical, chemical and adsorption properties. Microporous Mesoporous Mater 66:189–195. https://doi.org/10.1016/j.micromeso.2003.08.028
10. Alade AO, Amuda OS, Afolabi AO, Adelowo FE (2012) Adsorption of acenaphthene unto activated carbon produced from agricultural wastes. J Environ Sci Technol 5:192–202. https://doi.org/10.3923/jest.2012.192.209
11. Savova D, Apak E, Ekinci E et al (2001) Biomass conversion to carbon adsorbents and gas. Biomass Bioenergy 21:133–142. https://doi.org/10.1016/S0961-9534(01)00027-7
12. Rafatullah M, Sulaiman O, Hashim R, Ahmad A (2010) Adsorption of methylene blue on low-cost adsorbents: a review. J Hazard Mater 177:70–80. https://doi.org/10.1016/j.jhazmat.2009.12.047
13. Jin H, Capareda S, Chang Z et al (2014) Biochar pyrolytically produced from municipal solid wastes for aqueous As(V) removal: adsorption property and its improvement with KOH activation. Bioresour Technol 169C:622–629. https://doi.org/10.1016/j.biortech.2014.06.103
14. Peng P, Lang Y-H, Wang X-M (2016) Adsorption behavior and mechanism of pentachlorophenol on reed biochars: pH effect, pyrolysis temperature, hydrochloric acid treatment and isotherms. Ecol Eng 90:225–233. https://doi.org/10.1016/j.ecoleng.2016.01.039
15. Reza MS, Yun CS, Afroze S, Radenahmad N, Abu Bakar MS, Saidur R, Taweekun J, Azad AK (2020) Preparation of activated carbon from biomass and it's applications in water and gas purification, a review. Arab Journal of Basic and Applied Sciences 27(1): 208–238
16. Liu Z, Sun Y, Xu X, Meng X, Qu J, Wang Z, Liu C, Qu B (2020) Preparation, characterization and application of activated carbon from corn cob by KOH activation for removal of Hg(II) from aqueous solution. Bioresour Technol 306:123154

17. Wong S, Ngadi N, Inuwa IM, Hassan O (2018) Recent advances in applications of activated carbon from biowaste for wastewater treatment: a short review. J Clean Prod 175:361–375
18. Wang H, Xie R, Zhang J, Zhao J (2018) Preparation and characterization of distillers' grain based activated carbon as low cost methylene blue adsorbent: mass transfer and equilibrium modeling. Adv Powder Technol 29(1):27–35
19. Ahmed MJ (2016) Preparation of activated carbons from date (Phoenix dactylifera L.) palm stones and application for wastewater treatments: review. Process Saf Environ Prot 102:168–182
20. Anastopoulos I, Kyzas GZ (2014) Agricultural peels for dye adsorption: a review of recent literature. J Mol Liq 200:381–389
21. Gonzalez-Garcıa P (2018) Activated carbon from lignocellulosics precursors: a review of the synthesis methods, characterization techniques and applications. Renew Sust Energ Rev 82:1393–1414
22. Jeguirim M, Belhachemi M, Limousy L, Bennici S (2018) Adsorption/reduction of nitrogen dioxide on activated carbons: textural properties versus surface chemistry– a review. Chem Eng J Biochem Eng J 347:493–504
23. Green FJ (1990) The Sigma Aldrich Handbook of Stains, Dyes and Indicators. Milwaukee, Wisconsin: Aldrich Chemical Company, Inc., pp 461
24. Boutaieb M, Guiza M, Román Suero S et al (2020) Pine cone pyrolysis: optimization of temperature for energy recovery. Environ Prog Sustain Energy 39:e13272. https://doi.org/10.1002/ep.13272
25. Kaya N, Uzun Z (2020) Investigation of effectiveness of pyrolysis products on removal of alizarin yellow GG from aqueous solution: a comparative study with commercial activated carbon. Water Sci Technol 81(6):1191–1208. https://doi.org/10.2166/wst.2020.213
26. Creamer AE, Gao B, Wang S (2016) Carbon dioxide capture using various metal oxyhydroxide–biochar composites. Chem Eng J 283: 826–832. https://doi.org/10.1016/j.cej.2015.08.037
27. Saha P, Chowdhury S, Gupta S, Kumar I (2010) Insight into adsorption equilibrium, kinetics and thermodynamics of Malachite Green onto clayey soil of Indian origin. Chem Eng J 165:874–882. https://doi.org/10.1016/j.cej.2010.10.048
28. Martín-Lara MA, Blázquez G, Ronda A, Calero M (2016) Kinetic study of the pyrolysis of pine cone shell through non-isothermal thermogravimetry: effect of heavy metals incorporated by biosorption. Renew Energy 96:613–624. https://doi.org/10.1016/j.renene.2016.05.026
29. Cha JS, Park SH, Jung S-C et al (2016) Production and utilization of biochar: a review. J Ind Eng Chem 40:1–15. https://doi.org/10.1016/j.jiec.2016.06.002
30. Uzun BB, Yaman E (2017) Pyrolysis kinetics of walnut shell and waste polyolefins using thermogravimetric analysis. J Energy Inst 90:825–837. https://doi.org/10.1016/j.joei.2016.09.001
31. Liu Z, Singer S, Tong Y et al (2018) Characteristics and applications of biochars derived from wastewater solids. Renew Sust Energ Rev 90:650–664. https://doi.org/10.1016/j.rser.2018.02.040
32. Tan X, Liu S, Liu Y et al (2017) Biochar as potential sustainable precursors for activated carbon production: multiple applications in environmental protection and energy storage. Bioresour Technol 227:359–372. https://doi.org/10.1016/j.biortech.2016.12.083
33. Li S, Chen X, Liu A et al (2015) Co-pyrolysis characteristic of biomass and bituminous coal. Bioresour Technol 179:414–420. https://doi.org/10.1016/j.biortech.2014.12.025
34. Biswas S, Siddiqi H, Sen T et al (2020) Preparation and characterization of raw and inorganic acid-activated pine cone biochar and its application in the removal of aqueous-phase $Pb^{2+}$ metal ions by adsorption. Water, Air, Soil Pollut Focus 231:3. https://doi.org/10.1007/s11270-019-4375-7
35. Intergovernmental Panel on Climate Change (IPCC) (2018) Special Report of Global Warming of 1.5 °C
36. Kohlz AL, Nielsen RB (1997) Preface. In: Kohl AL, Nielsen RB (eds) Gas Purification, Fifth Edition. Gulf Professional Publishing, Houston, pp vii–viii
37. Anwar MN, Fayyaz A, Sohail NF et al (2018) $CO_2$ capture and storage: a way forward for sustainable environment. J Environ Manag 226:131–144. https://doi.org/10.1016/j.jenvman.2018.08.009
38. Koytsoumpa EI, Bergins C, Kakaras E (2018) The $CO_2$ economy: review of $CO_2$ capture and reuse technologies. J Supercrit Fluids 132:3–16. https://doi.org/10.1016/j.supflu.2017.07.029
39. Staciwa P, Narkiewicz U, Sibera D et al (2019) Carbon spheres as $CO_2$ sorbents. Appl Sci 9:3349. https://doi.org/10.3390/app9163349
40. Garg S, Das P (2019) Microporous carbon from cashew nutshell pyrolytic biochar and its potential application as $CO_2$ adsorbent. Biomass Convers Biorefinery. https://doi.org/10.1007/s13399-019-00506-1
41. Zhang X, Zhang S, Yang H et al (2015) Effects of hydrofluoric acid pre-deashing of rice husk on physicochemical properties and $CO_2$ adsorption performance of nitrogen-enriched biochar. Energy 91: 903–910. https://doi.org/10.1016/j.energy.2015.08.028
42. Manyà JJ, González B, Azuara M, Arner G (2018) Ultra-microporous adsorbents prepared from vine shoots-derived biochar with high $CO_2$ uptake and $CO_2/N_2$ selectivity. Chem Eng J 345: 631–639. https://doi.org/10.1016/j.cej.2018.01.092
43. Matabosch Coromina H, Walsh D, Mokaya R (2016) Biomass-derived activated carbon with simultaneously enhanced $CO_2$ uptake for both pre and post combustion capture applications. J Mater Chem A 4:280–289. https://doi.org/10.1039/C5TA09202G
44. Li D, Ma T, Zhang R et al (2015) Preparation of porous carbons with high low-pressure $CO_2$ uptake by KOH activation of rice husk char. Fuel 139:68–70. https://doi.org/10.1016/j.fuel.2014.08.027
45. Vargas DP, Giraldo L, Silvestre-Albero J, Moreno-Piraján JC (2011) $CO_2$ adsorption on binderless activated carbon monoliths. Adsorption 17:497–504. https://doi.org/10.1007/s10450-010-9309-z
46. Serafin J, Narkiewicz U, Morawski AW, et al (2017) Highly microporous activated carbons from biomass for $CO_2$ capture and effective micropores at different conditions. J $CO_2$ Util 18:73–79. https://doi.org/10.1016/j.jcou.2017.01.006
47. Deng S, Wei H, Chen T et al (2014) Superior $CO_2$ adsorption on pine nut shell-derived activated carbons and the effective micropores at different temperatures. Chem Eng J 253:46–54. https://doi.org/10.1016/j.cej.2014.04.115
48. Ghasemian Lemraski E, Sharafinia S (2016) Kinetics, equilibrium and thermodynamics studies of $Pb^{2+}$ adsorption onto new activated carbon prepared from Persian mesquite grain. J Mol Liq 219:482–492. https://doi.org/10.1016/j.molliq.2016.03.031
49. Atas MS, Dursun S, Akyildiz H et al (2017) Selective removal of cationic micro-pollutants using disulfide-linked network structures. RSC Adv 7:25969–25977. https://doi.org/10.1039/C7RA04775D
50. Al-Rubayee WT, Abdul-Rasheed OF, Ali NM (2016) Preparation of a modified nanoalumina sorbent for the removal of alizarin yellow R and methylene blue dyes from aqueous solutions. J Chem 2016:4683859. https://doi.org/10.1155/2016/4683859
51. Rattanapan S, Srikram J, Kongsune P (2017) Adsorption of methyl orange on coffee grounds activated carbon. Energy Procedia 138: 949–954. https://doi.org/10.1016/j.egypro.2017.10.064
52. Yakout S, Hassan M, El-Zaidy M et al (2020) Kinetic study of methyl orange adsorption on activated carbon derived from pine (pinus strobus) sawdust. Bioresources 14:4560–4574
53. Moreno-Castilla C (2004) Adsorption of organic molecules from aqueous solutions on carbon materials. Carbon N Y 42:83–94. https://doi.org/10.1016/j.carbon.2003.09.022
54. Chowdhury S, Chakraborty S, Saha P (2011) Biosorption of Basic Green 4 from aqueous solution by Ananas comosus (pineapple) leaf

powder. Colloids Surf B: Biointerfaces 84:520–527. https://doi.org/10.1016/j.colsurfb.2011.02.009
55. Changmai M, Banerjee P, Nahar K, Purkait MK (2018) A novel adsorbent from carrot, tomato and polyethylene terephthalate waste as a potential adsorbent for Co (II) from aqueous solution: kinetic and equilibrium studies. J Environ Chem Eng 6:246–257. https://doi.org/10.1016/j.jece.2017.12.009
56. Chen J, Shi X, Zhan Y et al (2017) Construction of horizontal stratum landform-like composite foams and their methyl orange adsorption capacity. Appl Surf Sci 397:133–143. https://doi.org/10.1016/j.apsusc.2016.10.211
57. Gao M, Ma Q, Lin Q et al (2015) Combined modification of fly ash with $Ca(OH)_2$/$Na_2FeO_4$ and its adsorption of methyl orange. Appl Surf Sci 359:323–330. https://doi.org/10.1016/j.apsusc.2015.10.135
58. Martini BK, Daniel TG, Corazza MZ, de Carvalho AE (2018) Methyl orange and tartrazine yellow adsorption on activated carbon prepared from boiler residue: kinetics, isotherms, thermodynamics studies and material characterization. J Environ Chem Eng 6:6669–6679. https://doi.org/10.1016/j.jece.2018.10.013
59. León G, García F, Miguel B, Bayo J (2016) Equilibrium, kinetic and thermodynamic studies of methyl orange removal by adsorption onto granular activated carbon. Desalin Water Treat 57(36): 17104–17117. https://doi.org/10.1080/19443994.2015.1072063
60. Kumar V, Srinivas G, Wood B et al (2019) Characterization of adsorption site energies and heterogeneous surfaces of porous materials. J Mater Chem A 7:10104–10137. https://doi.org/10.1039/C9TA00287A
61. Doğan M, Abak H, Alkan M (2009) Adsorption of methylene blue onto hazelnut shell: kinetics, mechanism and activation parameters. J Hazard Mater 164:172–181. https://doi.org/10.1016/j.jhazmat.2008.07.155
62. Mahmoudi K, Hamdi N, Kriaa A, Srasra E (2012) Adsorption of methyl orange using activated carbon prepared from lignin by $ZnCl_2$ treatment. Russ J Phys Chem A 86:1294–1300. https://doi.org/10.1134/S0036024412060180
63. Yönten V, Sanyürek NK, Kivanç MR (2020) A thermodynamic and kinetic approach to adsorption of methyl orange from aqueous solution using a low cost activated carbon prepared from Vitis vinifera L. Surfaces and Interfaces 20:100529. https://doi.org/10.1016/j.surfin.2020.100529
64. Subbaiah MV, Kim D-S (2016) Adsorption of methyl orange from aqueous solution by aminated pumpkin seed powder: kinetics, isotherms, and thermodynamic studies. Ecotoxicol Environ Saf 128: 109–117. https://doi.org/10.1016/j.ecoenv.2016.02.016
65. Goldfarb JL, Ceylan S (2015) Second-generation sustainability: application of the distributed activation energy model to the pyrolysis of locally sourced biomass–coal blends for use in co-firing scenarios. Fuel 160:297–308. https://doi.org/10.1016/j.fuel.2015.07.071
66. Liu G, Song H, Wu J (2015) Thermogravimetric study and kinetic analysis of dried industrial sludge pyrolysis. Waste Manag 41:128–133. https://doi.org/10.1016/j.wasman.2015.03.042
67. Odeh AO (2015) Oualitative and quantitative ATR-FTIR analysis and its application to coal char of different ranks. J Fuel Chem Technol 43:129–137. https://doi.org/10.1016/S1872-5813(15)30001-3
68. Plis A, Lasek J, Skawińska A, Zuwała J (2015) Thermochemical and kinetic analysis of the pyrolysis process in Cladophora glomerata algae. J Anal Appl Pyrolysis 115:166–174. https://doi.org/10.1016/j.jaap.2015.07.013
69. Yorgun S, Yıldız D (2015) Preparation and characterization of activated carbons from Paulownia wood by chemical activation with $H_3PO_4$. J Taiwan Inst Chem Eng 53:122–131. https://doi.org/10.1016/j.jtice.2015.02.032